

INTRINSIC LOCAL GAUSS'S LAW PRESERVING PIC METHOD: A SELF-CONSISTENT FIELD-PARTICLE UPDATE SCHEME FOR PLASMA SIMULATIONS

ZHONGHUA QIAO*, ZHENLI XU [†], QIAN YIN [‡], AND SHENGGAO ZHOU[§]

Abstract. In order to perform physically faithful particle-in-cell (PIC) simulations, the Gauss's law stands as a critical requirement, since its violation often leads to catastrophic errors in long-term plasma simulations. This work proposes a novel method that intrinsically enforces the Gauss's law for the Vlasov-Ampère/Vlasov-Poisson system without requiring auxiliary field corrections or specialized current deposition techniques. The electric field is managed to get updated locally and consistently with the motion of particles via splitting the motion into sub-steps along each dimension of the computational mesh. To further obtain a curl-free electric field, a local update scheme is developed to relax the electric-field free energy subject to the Gauss's law. The proposed method avoids solving the Poisson's or Ampère's equation, resulting in a local algorithm of linear complexity for each time step which can be flexibly combined with various temporal discretization for particle motion in PIC simulations. Theoretical analysis verifies that the proposed method indeed maintains the discrete Gauss's law exactly. Numerical tests on classical benchmarks, including the Landau damping, two-stream instability and Diocotron instability, demonstrate the key advantages of the proposed method. It is expected that the local nature of the proposed method makes it a promising tool in parallel simulations of large-scale plasmas.

Key words and phrases: Gauss's law preservation, Particle-in-cell (PIC), Local relaxation, Field-particle update

MSC codes: 65Z05 65M75 35Q83

1. Introduction. The Vlasov equation is a kinetic equation describing the evolution of charged particles under electromagnetic fields [13]. It differs slightly from the Boltzmann equation [24], neglecting short-range collisions and emphasizing on interactions governed by self-consistent fields. In the complete electromagnetic formulation, the Vlasov equation is coupled with the full set of Maxwell's equations, where the electric and magnetic field can be solved using charge densities and currents generated by particle motions. Under electrostatic approximations, this framework reduces to two equivalent formulations [8, 33], the Vlasov-Poisson system, computing electric field via Poisson's equation, and Vlasov-Ampère system, deriving electric field from Ampère's equation under local charge continuity equation, both neglecting magnetic effects.

While analytical solutions exist only for idealized systems, such as the linear waves; therefore, numerical methods become necessary in order to study the phenomenon governed by the Vlasov equation. Overall, these numerical methods can be broadly classified into two categories: Eulerian approaches, which involve direct solutions of the Vlasov equation, and particle-based methods, in which the distribution is approximated through discrete macro-particles. The Eulerian methods, including the discontinuous Galerkin [11], finite volume [19], semi-Lagrangian [36, 52], moment methods [60] and so on [23, 27], are suitable for high-precision phase-space analysis, whereas the Particle-in-Cell (PIC) method [4, 28, 30, 44], belonging to particle-based

*Department of Applied Mathematics, the Hong Kong Polytechnic University, Hong Kong, China. (zhonghua.qiao@polyu.edu.hk)

[†]School of Mathematical Sciences, MOE-LSC, and CMA-Shanghai, Shanghai Jiao Tong University, Shanghai 200240, China. (xuzl@sjtu.edu.cn)

[‡]Corresponding author. Department of Applied Mathematics, the Hong Kong Polytechnic University, Hong Kong, China. (qqian.yin@polyu.edu.hk)

[§]School of Mathematical Sciences, MOE-LSC, and CMA-Shanghai, Shanghai Jiao Tong University, Shanghai 200240, China. (sgzhou@sjtu.edu.cn)

methods, dominates high-dimensional, large-scale simulations due to its computational scalability. Some works use phase-space remapping to reduce the numerical noise in PIC simulations to obtain higher accuracy [46, 62]. There are also many attempts to prove the convergence of particle methods for the Vlasov equation coupled with the Poisson’s equation [14, 48].

Preserving critical mathematical and physical properties in PIC simulations is essential and highly desirable for ensuring the accuracy and reliability of numerical results, especially in long-term simulations. For instance, asymptotic-preserving (AP) schemes [16, 25] that are able to maintain cross-scale consistency have been shown to be indispensable in resolving multiscale coupling challenges when the Debye length approaches the quasi-neutral limit. Also, the total energy, which comprises contributions from electric field energy and kinetic energy, should theoretically remain conservative in continuous systems. But finite-grid instabilities can induce unphysical heating or cooling phenomena. This has motivated extensive development of energy-conserving schemes [7, 6, 9, 31, 54, 55]. Additionally, momentum-conserving methods [12, 41] are desirable as well. Among the various conservation requirements, mass conservation and the Gauss’s law form the cornerstones of robust PIC simulations, and have been critically addressed in the aforementioned studies. Significantly, as shall be shown in Section 2.3, the design of local mass conservation inherently helps the preservation of the Gauss’s law. As highlighted by Anderson *et al.* [1], failure to enforce the Gauss’s law can lead to catastrophic consequences in PIC simulations.

This study proposes an intrinsic local Gauss’s law-preserving PIC framework that can be strategically combined with additional conservation-enforcing methods to achieve comprehensive conservation properties for the Vlasov-Ampère systems. Recent progress on the enforcement of the Gauss’s law, which is systematically reviewed in Section 2.3, fall into two distinct categories: field correction methods [5, 29, 40, 45] that post-process the electric field to eliminate inconsistencies in the Gauss’s law, and charge-conserving methods [43, 58, 61] that enforce discrete continuity equations through carefully designed current densities. This work proposes a novel Gauss’s law-preserving framework that fundamentally differs from these conventional approaches. The proposed algorithm achieves this through a unified field-particle advancement scheme that simultaneously updates electric fields and particle positions while strictly maintaining the discrete Gauss’s law up to machine precision. More specifically, the electric field is locally updated to account for electric fluxes induced by the particle motion along the trajectory of motion, and then these updates further diffuse to the whole area through a local curl-free relaxation approach aiming to minimize the electric field free energy. The whole process eliminates explicit dependence on the Poisson or Ampère solvers through its self-consistent treatment of field propagation and particle dynamics. Such type of local algorithms is firstly proposed for Monte Carlo simulations [37, 38, 56], as well as the molecular dynamics simulations [17, 18, 47, 57] for electrostatic systems. Later, it was further generalized to solve continuum electrostatic models, such as the Poisson-Boltzmann equation [2, 51, 64] and Poisson-Nernst-Planck equations [49, 50]. The distinctive features on the preservation of the Gauss’s law and inherent locality makes the proposed method particularly advantageous for plasma simulations where simultaneous conservation of multiple properties (mass, momentum, energy) is crucial.

The rest of this paper is organized as follows. Section 2 provides an overview of Vlasov type of models and PIC methods, and reviews related works on the treatment of electric fields that preserve the Gauss’s law. In Section 3, we elaborate on the proposed local Gauss’s law preserving PIC methods. Some numerical experiments

are conducted in Section 4. Finally, conclusions are summarized in Section 5.

2. Model and numerical methods.

2.1. Vlasov-Ampère equations. The Vlasov equation, often used to describe inertial confinement fusion, astrophysics and so on, is given by

$$\frac{\partial f_s(\mathbf{x}, \mathbf{v}, t)}{\partial t} + \mathbf{v} \cdot \nabla_{\mathbf{x}} f_s(\mathbf{x}, \mathbf{v}, t) + \mathbf{F}(\mathbf{x}, t) \cdot \nabla_{\mathbf{v}} f_s(\mathbf{x}, \mathbf{v}, t) = 0,$$

where $f_s(\mathbf{x}, \mathbf{v}, t)$ represents the distribution of particles of species s at a specific position \mathbf{x} , velocity \mathbf{v} and time t . Here $\mathbf{F}(\mathbf{x}, t)$ is the external force. Generally, the force field includes electrostatic and Lorentz force, i.e. $\mathbf{F}(\mathbf{x}, t) = q_s(\mathbf{E} + \mathbf{v} \wedge \mathbf{B})/m_s$, where q_s is charge carried by particles, m_s is mass, and the electric field \mathbf{E} and magnetic field \mathbf{B} are described by the Maxwell's equation

$$(2.1) \quad \frac{\partial \mathbf{E}}{\partial t} - c^2 \nabla \times \mathbf{B} = -\frac{\mathbf{J}}{\epsilon_0},$$

$$(2.2) \quad \frac{\partial \mathbf{B}}{\partial t} + \nabla \times \mathbf{E} = 0,$$

$$(2.3) \quad \nabla \cdot \mathbf{E} = \frac{\rho}{\epsilon_0},$$

$$(2.4) \quad \nabla \cdot \mathbf{B} = 0.$$

Here c is the speed of light, ϵ_0 is the vacuum permittivity, $\rho(\mathbf{x}, t)$ the charge density and $\mathbf{J}(\mathbf{x}, t)$ the current density are expressed by

$$\rho(\mathbf{x}, t) = \sum_s q_s \int_{\Omega_v} f_s d\mathbf{v}, \quad \mathbf{J}(\mathbf{x}, t) = \sum_s q_s \int_{\Omega_v} f_s \mathbf{v} d\mathbf{v},$$

respectively.

In this work, we consider the electrostatic limit. The above Vlasov-Maxwell model can be approximated by the Vlasov-Poisson (VP) model, in which the force becomes $\mathbf{F}(t, \mathbf{x}) = q_s \mathbf{E}/m_s$ with $\mathbf{E} = -\nabla \phi$. The electric potential ϕ is governed by the Poisson's equation

$$-\nabla \cdot \nabla \phi(\mathbf{x}, t) = \rho/\epsilon_0.$$

By integrating the Vlasov equation with respect to the velocity field and summing over s , one gets the charge continuity equation

$$(2.5) \quad \frac{\partial \rho(\mathbf{x}, t)}{\partial t} + \nabla \cdot \mathbf{J}(\mathbf{x}, t) = 0.$$

By the Gauss's law (2.3), one gets

$$\nabla \cdot \left[\epsilon_0 \frac{\partial \mathbf{E}}{\partial t} + \mathbf{J} \right] = 0.$$

Therefore, the electric field \mathbf{E} can be described by the Ampère's equation (2.1)

$$(2.6) \quad \epsilon_0 \frac{\partial \mathbf{E}}{\partial t} + \mathbf{J} = \mathbf{Q},$$

where \mathbf{Q} is an extra freedom satisfying a divergence free condition $\nabla \cdot \mathbf{Q} = 0$. Coupling (2.6) and the curl-free condition $\nabla \times \mathbf{E} = 0$ with the Vlasov equation gives the Vlasov-Ampère (VA) model.

In the continuum, the VP and VA formulations can be shown to be equivalent [8, 33]. Above derivation also reveals that the charge continuity equation (2.5) and Gauss's law (2.3) play critical roles in conversion between the VP and VA formulations.

We perform non-dimensionalization, as detailed in [33], and still take the original variables without causing any ambiguity. For the sake of descriptive convenience, we consider the Vlasov equation with only one specie, i.e. electron:

$$(2.7) \quad \frac{\partial f(\mathbf{x}, \mathbf{v}, t)}{\partial t} + \mathbf{v} \cdot \nabla_{\mathbf{x}} f(\mathbf{x}, \mathbf{v}, t) - \mathbf{E}(\mathbf{x}, t) \cdot \nabla_{\mathbf{v}} f(\mathbf{x}, \mathbf{v}, t) = 0.$$

The non-dimensionalized Poisson's equation and Ampère's equation are given by

$$-\nabla \cdot \lambda^2 \nabla \phi(\mathbf{x}, t) = \rho = n_0 - n, \quad \mathbf{E} = -\nabla \phi,$$

and

$$\lambda^2 \frac{\partial \mathbf{E}}{\partial t} + \mathbf{J} = \mathbf{Q}, \quad \nabla \cdot \mathbf{Q} = 0, \quad \nabla \times \mathbf{E} = 0,$$

respectively, where λ is ratio of the Debye length to the characteristic length of the system under consideration, n_0 is the density of background ion, and

$$n(\mathbf{x}, t) = - \int_{\Omega_v} f_s d\mathbf{v}, \quad \text{and} \quad \mathbf{J}(\mathbf{x}, t) = - \int_{\Omega_v} f_s \mathbf{v} d\mathbf{v}.$$

2.2. Particle-in-cell method. The PIC method is a widely used numerical technique for simulating the Vlasov equations for plasma dynamics. It combines the motion of charged particles with the evolution of electromagnetic fields, making it a powerful tool for tackling the high-dimension challenge in the simulation of a variety of plasma phenomena. In the PIC method, the distribution function f is approximated by

$$(2.8) \quad f(\mathbf{x}, \mathbf{v}, t) = \sum_{p=1}^{N_p} w_p S(\mathbf{x} - \mathbf{x}_p) \delta(\mathbf{v} - \mathbf{v}_p),$$

where N_p is the number of computational particles, $\delta(\mathbf{v} - \mathbf{v}_p)$ is the Dirac delta function, and w_p is the weight of the p -th particle defined by the ratio of numbers of real physical particles to computational particles and is often treated as a constant in collisionless PIC simulations. In addition, $S(\mathbf{x} - \mathbf{x}_p)$ is the shape function that has a particular compact support, is symmetric, and integrates to 1, i.e. $\int_{\Omega_x} S(\mathbf{x}) d\mathbf{x} = 1$. It can be chosen as the B-spline, Gaussian functions or others. The most commonly used shape function in 1D is the “tent” function, defined as $S(x) = \max\{0, 1 - |x|/h\}/h$, where h is the grid spacing. The shape function in higher dimensions is obtained by taking the product of 1D ones, e.g., $S(x, y, z) = S_x(x)S_y(y)S_z(z)$. Substituting the particle approximation (2.8) into the Vlasov equation (2.7), one can obtain the evolution equation for the particles from the first-order momentum of the Vlasov equation [30]:

$$(2.9) \quad \frac{d\mathbf{x}_p}{dt} = \mathbf{v}_p,$$

$$(2.10) \quad \frac{d\mathbf{v}_p}{dt} = -\mathbf{E}(\mathbf{x}_p),$$

for $p = 1, \dots, N_p$. The mobile particles follow the above Newton's law, which imparts a “granular” nature. Meanwhile, the potential and electric field are represented by

values on a regular mesh of grid points, necessitating the projection of discrete values defined on the grid points onto the distribution of particles, and vice versa. Densities defined on the mesh are calculated by assigning the particle charge to nearby mesh points:

$$(2.11) \quad n_h(t) = \sum_{p=1}^{N_p} \omega_p S(\mathbf{x}_h - \mathbf{x}_p(t)),$$

where the subscript h indicates that the quantity is defined on the mesh. Similarly, for currents,

$$(2.12) \quad \mathbf{J}_h(t) = - \sum_{p=1}^{N_p} \omega_p S(\mathbf{x}_h - \mathbf{x}_p(t)) \mathbf{v}_p(t).$$

With densities $n_h(t)$ and currents $\mathbf{J}_h(t)$, field \mathbf{E}_h defined on mesh can be computed using the Poisson's equation or Ampère's equation. Then, potentials and fields at particle positions are further obtained by interpolating the mesh-defined values by

$$\mathbf{E}(\mathbf{x}_p) = |\Delta V| \sum_h \mathbf{E}_h(t) S(\mathbf{x}_h - \mathbf{x}_p(t)),$$

where $|\Delta V|$ is the volume of a single cell.

In PIC simulations of plasma, it is necessary to obtain accurate spatial distribution of potential and electric fields, ensuring proper treatment of particle dynamics. The motion of particles can in turn cause global changes of the fields in the system. Therefore, even minute particle movement requires recalculating the Poisson's equation globally at each time step, which accounts for the vast majority of the total computational effort. The update method proposed in this work ensures rapid and accurate acquisition of the desired electric fields by concurrently updating the particle positions and the electric field, while rigorously adhering to the Gauss's law.

2.3. Gauss's law and charge conservation. The Gauss's law (2.3), which states that the divergence of the electric field is proportional to the charge density, is a fundamental principle of electromagnetism. In PIC simulations, accurate enforcement of the Gauss's law ensures that the electric field is correctly coupled with the charge distribution, being essential for modeling the interactions between particles and fields. In this section, we emphasize the importance of the Gauss's law in PIC simulations and review various methods from the literature devoted to satisfy the Gauss's law, highlighting the advantage of our algorithm in naturally fulfilling the law.

One class of methods is to correct the electric field to enforce the Gauss's law by adding a correction term. The well-known Boris correction [5, 4] introduces an extra term $\delta\phi$ so that the corrected electric field $\mathbf{E}_{\text{correct}} = \mathbf{E} - \nabla\delta\phi$ satisfies the Gauss's law $\nabla \cdot \varepsilon \mathbf{E}_{\text{correct}} = \rho$. Hence, solving the Poisson's equation,

$$\nabla \cdot \varepsilon \nabla \delta\phi = \nabla \cdot \varepsilon \mathbf{E} - \rho,$$

is needed in the Boris correction method. Later, Marder [40] and Langdon [29] proposed an alternative type of method through replacing the Poisson solver by a local update of electric fields

$$\mathbf{E}_{\text{correct}}^{n+1} = \mathbf{E}^{n+1} + \Delta t \nabla [d(\nabla \cdot \varepsilon \mathbf{E} - \rho)],$$

where d is the diffusion parameter satisfying a stability condition [29, 39]. Later, Munz *et al.* generalized this idea into a framework of the Lagrange multiplier method [45]. Recently, Chen and Tóth [10] proposed a series of particle position correction methods to realize the Gauss's law, taking into account the trade-off between computational cost and the tolerance error of the Gauss's law. Different from the previous, such methods correct the displacement of particles to ensure that the energy conservation property is not violated, especially when combined with energy conserving semi-implicit methods [31].

The global charge conservation law, which describes that the total charge in the system remains constant, is crucially important as well. The particle method used in this work naturally preserves this global law. In literature, density or current is designed to fulfill the discrete version of the local charge conservation equation (2.5) and therefore satisfy the Gauss's law. The rationale behind this is detailed as follows. Consider certain temporal discretization

$$\epsilon_0 \frac{\mathbf{E}_h^{n+1} - \mathbf{E}_h^n}{\Delta t} + \mathbf{J}_h^* = \mathbf{Q}_h^*,$$

where the superscript $*$ indicates an either implicit or explicit discretization time step. Taking spatial divergence on the both sides yields

$$\epsilon_0 \nabla_h \cdot \frac{\mathbf{E}_h^{n+1} - \mathbf{E}_h^n}{\Delta t} + \nabla_h \cdot \mathbf{J}_h^* = 0,$$

where ∇_h is the discrete analog of the operator ∇ and shall be detailed in Section 3.1. By the discrete charge conserving law

$$(2.13) \quad \frac{\rho_h^{n+1} - \rho_h^n}{\Delta t} + \nabla_h \cdot \mathbf{J}_h^* = 0,$$

one can obtain

$$\epsilon_0 \nabla_h \cdot \frac{\mathbf{E}_h^{n+1} - \mathbf{E}_h^n}{\Delta t} + \frac{\rho_h^{n+1} - \rho_h^n}{\Delta t} = 0.$$

Therefore, one can readily derive that provided by the Gauss's law at time $n\Delta t$ is valid, the discrete charge conserving law and the Gauss's law at time $(n+1)\Delta t$ are equivalent. Substituting the expressions (2.11) and (2.12) with the shape function into (2.13), one gets

$$\frac{S(\mathbf{x}_h - \mathbf{x}_p^{n+1}) - S(\mathbf{x}_h - \mathbf{x}_p^n)}{\Delta t} + \nabla_h \cdot [\mathbf{v}_p^* S(\mathbf{x}_h - \mathbf{x}_p^*)] = 0,$$

which is the basis for most “current weighting” methods [43, 61, 58]. In PIC simulations, the charge conserving law may get violated when a particle crosses cell boundaries. The particle motion can be split into sub-steps to restrict the particle moving within one cell, so that the exact charge conservation can be achieved [8, 6].

3. Local Gauss's law preserving PIC method.

3.1. Discretization. The classical temporal discretization for particle motion equations (2.9)–(2.10) in the PIC is the so-called “leapfrog” scheme, where positions are defined at integer values of the time-step, i.e., $\mathbf{x}_p^m = \mathbf{x}_p(m\Delta t)$, while velocities are defined at half-integer values: $\mathbf{v}_p^{m+1/2} = \mathbf{v}_p((m+1/2)\Delta t)$. They are alternately

updated in the following manner:

$$(3.1) \quad \mathbf{x}^{m+1} = \mathbf{x}^m + \Delta t \mathbf{v}^{m+\frac{1}{2}},$$

$$(3.2) \quad \mathbf{v}^{m+\frac{3}{2}} = \mathbf{v}^{m+\frac{1}{2}} - \Delta t \mathbf{E}^{m+1}(\mathbf{x}_p),$$

where $\mathbf{E}^{m+1}(\mathbf{x}_p) = \mathbf{E}(\mathbf{x}_p^{m+1})$ is the electric field interpolated using grid data. The initial velocity at a half time step is obtained using an explicit scheme

$$\mathbf{v}^{\frac{1}{2}} = \mathbf{v}^0 - \frac{1}{2} \Delta t \mathbf{E}^0(\mathbf{x}_p).$$

Such staggered updating of positions and velocities over time steps gives its name leapfrog. Meanwhile, this explicit scheme has several advantages, such as second-order accuracy, computational simplicity, and preservation of phase space volume, making it suitable for long-term simulations of Hamiltonian systems.

For spatial discretization, we adopt the standard finite-difference Yee mesh [63, 59], in which scalar quantities, such as potential and charge density, are discretized on grid points of cells, while the electric fields are discretized at the center of cell edges. Consider a square computational domain $\Omega_x = [0, L] \times [0, L]$ with periodic boundary conditions. The domain is covered with a uniform mesh with grid spacing $h = L/(N-1)$ in each dimension. Specifically, let $n_{i,j}$ ($i, j = 0, \dots, N-1$) be the numerical approximation of density n on the grid point (ih, jh) , and $E_{i+1/2,j}$ and $E_{i,j+1/2}$ are discrete analogues of the projected values of electric fields at midpoints of the edges $((i+1/2)h, jh)$ and $(ih, (j+1/2)h)$, respectively. With the Yee mesh, the Gauss's law is approximated by

$$(3.3) \quad \frac{E_{i+\frac{1}{2},j} - E_{i-\frac{1}{2},j}}{h} + \frac{E_{i,j+\frac{1}{2}} - E_{i,j-\frac{1}{2}}}{h} = \frac{n_0 - n_{i,j}}{\lambda^2}.$$

It has been shown that such spatial discretization has second order accuracy for the electric field in both L^∞ and L^2 norms [32].

3.2. Particle motion with electric-field update. As demonstrated in Section 2.3, it is crucial to satisfy the Gauss's law for long-term simulations. The change in the electric field depends on the evolution of charge density, which in turn determines particle motion. We here propose a novel algorithm that updates the electric field simultaneously with particle motion, ensuring that Gauss's law is satisfied within machine precision. For simplicity, the algorithm is presented in 2D and can be extended in a straightforward manner to 3D. Let particle position $\mathbf{x}_p = (x_{p,x}, x_{p,y})$ and velocity $\mathbf{v}_p = (v_{p,x}, v_{p,y})$. When the particle positions get updated according to the "leapfrog" scheme (3.1), we update the locations of particles parallel to the links of the mesh in the following two steps

$$(3.4) \quad x_{p,x}^{m+1} = x_{p,x}^m + \Delta t v_{p,x}^{m+\frac{1}{2}},$$

$$(3.5) \quad x_{p,y}^{m+1} = x_{p,y}^m + \Delta t v_{p,y}^{m+\frac{1}{2}}.$$

As shown in Figure 1 (a), the particle motion from $\mathbf{x}_p^m = (x_{p,x}^m, x_{p,y}^m)$ to $\mathbf{x}_p^{m+1} = (x_{p,x}^{m+1}, x_{p,y}^{m+1})$ within one timestep is split into two orthogonal moves: first \mathbf{x}_p^m to $(x_{p,x}^{m+1}, x_{p,y}^m)$, and then to \mathbf{x}_p^{m+1} .

After updating the position of each particle along each direction, the electric field along the path of motion in that direction is also immediately updated to satisfy the

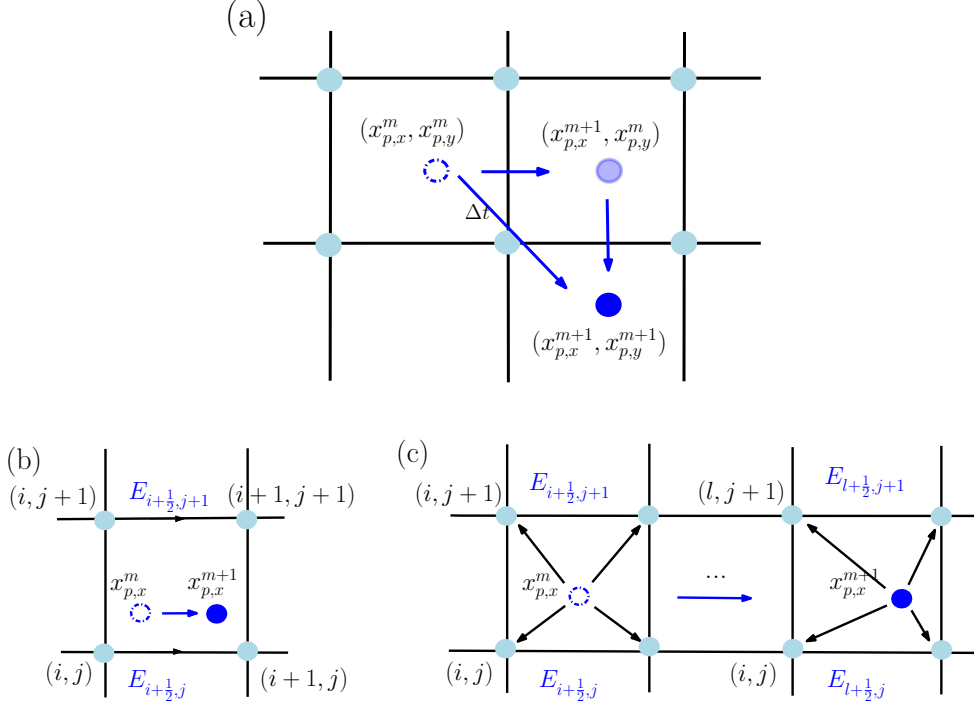


Fig. 1: Electric-field update with particle motion. (a) The particle motion is split into two orthogonal moves. (b) Update \mathbf{E} based on Gauss's law within one cell. (c) Update \mathbf{E} based on Gauss's law when crossing the cell boundary.

Gauss's law. For simplicity, we consider the support of the shape function S as $[0, h]^2$. Consider one particle that moves from point $\mathbf{x}_p^m = (x_{p,x}^m, x_{p,y}^m)$ to point $(x_{p,x}^{m+1}, x_{p,y}^{m+1})$ in x direction as in (3.4). There exists a pair of index (i, j) , such that $ih \leq x_{p,x}^m < (i+1)h$ and $jh \leq x_{p,y}^m < (j+1)h$. Let us first assume that the movement distance is small enough so that the updated position is still within the same cell (cf. Figure 1 (b)), meaning that $ih \leq x_{p,x}^{m+1} < (i+1)h$. Define the distances

$$d_{x,i}^m = |ih - x_{p,x}^m| \quad \text{and} \quad d_{y,j}^m = |jh - x_{p,y}^m|.$$

Such movement causes the corresponding electric field $E_{i+1/2,j}$ and $E_{i,j+1/2}$ changed by

$$E_{i+1/2,j}^* \leftarrow E_{i+1/2,j} - \frac{1}{\lambda^2} h w_p [S_x(d_{x,i}^{m+1}) - S_x(d_{x,i}^m)] S_y(d_{y,j}^m),$$

$$E_{i+1/2,j+1}^* \leftarrow E_{i+1/2,j+1} - \frac{1}{\lambda^2} h w_p [S_x(d_{x,i}^{m+1}) - S_x(d_{x,i}^m)] S_y(d_{y,j+1}^m).$$

If the movement distance is larger and the particle crosses the cell boundary, there exists an integer l such that $lh \leq x_{p,x}^{m+1} < (l+1)h$; cf. Figure 1 (c). Here we assume $l > i$. The other case $l < i$ can be treated similarly. All relevant electric fields along the path, i.e. $E_{i+1/2,j}, \dots, E_{l+1/2,j}$ and $E_{i+1/2,j+1}, \dots, E_{l+1/2,j+1}$ are updated

accordingly based on the Gauss's law (3.3):

$$(3.6) \quad E_{i+\frac{1}{2},j}^* \leftarrow E_{i+\frac{1}{2},j} - \frac{1}{\lambda^2} h w_p [-S_x(d_{x,i}^m)] S_y(d_{y,j}^m),$$

$$(3.7) \quad E_{i+\frac{1}{2},j+1}^* \leftarrow E_{i+\frac{1}{2},j+1} - \frac{1}{\lambda^2} h w_p [-S_x(d_{x,i}^m)] S_y(d_{y,j+1}^m),$$

$$(3.8) \quad E_{r+\frac{1}{2},j}^* \leftarrow E_{r+\frac{1}{2},j} - \frac{1}{\lambda^2} h w_p [-S_x(d_{x,i}^m) + S_x(d_{x,i+1}^{m+1}) - S_x(d_{x,i+1}^m)] S_y(d_{y,j}^m),$$

$$(3.9) \quad E_{r+\frac{1}{2},j+1}^* \leftarrow E_{r+\frac{1}{2},j+1} - \frac{1}{\lambda^2} h w_p [-S_x(d_{x,i}^m) + S_x(d_{x,i+1}^{m+1}) - S_x(d_{x,i+1}^m)] S_y(d_{y,j+1}^m),$$

for $r = i + 1, \dots, l - 1$, and

$$(3.10) \quad E_{l+\frac{1}{2},j}^* \leftarrow E_{l+\frac{1}{2},j} + \frac{1}{\lambda^2} h w_p [S_x(d_{x,l+1}^{m+1})] S_y(d_{y,j}^m),$$

$$(3.11) \quad E_{l+\frac{1}{2},j+1}^* \leftarrow E_{l+\frac{1}{2},j+1} + \frac{1}{\lambda^2} h w_p [S_x(d_{x,l+1}^{m+1})] S_y(d_{y,j+1}^m).$$

The motions in other directions (3.5), moving from point $(x_{p,x}^{m+1}, x_{p,y}^m)$ to $\mathbf{x}_p^{m+1} = (x_{p,x}^{m+1}, x_{p,y}^{m+1})$, are treated similarly. By doing so, we maintain the Gauss's law strictly by updating the electric field simultaneously with the particle motion, instead of solving the Poisson's or Ampère's equation.

3.3. Electric field correction. After above updates, there is one more condition that needs to be satisfied: the curl-free condition of the electric field. This condition can be achieved through a local curl-free relaxation algorithm that is of linear complexity [38, 49]. The starting point of the local relaxation algorithm is to minimize a convex electrostatic free energy

$$\mathcal{F}_{\text{pot}}(\mathbf{E}) = \lambda^2 \int_{\Omega} \mathbf{E}^2 / 2 \, d\mathbf{x},$$

subject to the constraint of the Gauss's law (2.3). It can be shown by the Lagrange multiplier method that the unique minimizer of the constrained optimization problem is the desired solution satisfying the curl-free condition [49]. After the updates in the previous section, we obtain Gauss's law satisfying fields \mathbf{E}_h^* , which shall be labeled as $\mathbf{E}_h^{(0)}$. In this section, we shall develop a Gauss's law preserving iterative method to minimize the free energy so that it approaches curl free on the Gauss's law preserving manifold.

The first step of correction involves looping over all the cells in the computational mesh. Let us take one cell as an example, as shown in Figure 2 (a). We increase the electric field components $E_{i+1/2,j}$ and $E_{i+1,j+1/2}$ by a small increment η , while decrease $E_{i+1/2,j+1}$ and $E_{i,j+1/2}$ by η :

$$(3.12) \quad \begin{aligned} E_{i+\frac{1}{2},j}^{(q+1)} &\leftarrow E_{i+\frac{1}{2},j}^{(q)} + \eta, & E_{i+1,j+\frac{1}{2}}^{(q+1)} &\leftarrow E_{i+1,j+\frac{1}{2}}^{(q)} + \eta, \\ E_{i+\frac{1}{2},j+1}^{(q+1)} &\leftarrow E_{i+\frac{1}{2},j+1}^{(q)} - \eta, & E_{i,j+\frac{1}{2}}^{(q+1)} &\leftarrow E_{i,j+\frac{1}{2}}^{(q)} - \eta, \end{aligned}$$

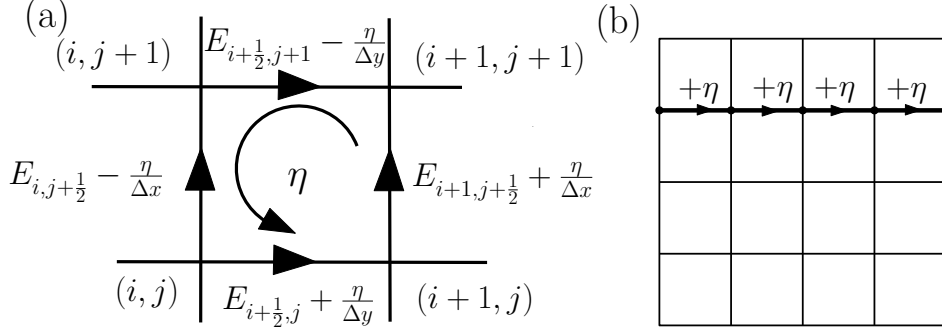


Fig. 2: The correction of the electric field. (a): Local curl-free relaxation. (b): Line shift.

where the superscript q denotes the iteration step in this correction phase. It is straightforward to check that the total fluxes entering and leaving each one of the four involved vertices remain unchanged, maintaining the Gauss's law on these four vertices. The associated change in the free energy due to the update of electric fields reads

$$\delta \mathcal{F}_{\text{pot}}^h[\eta] = 2\lambda^2 \eta^2 + \lambda^2 \eta \left[\left(E_{i+\frac{1}{2},j}^{(q)} - E_{i+\frac{1}{2},j+1}^{(q)} \right) + \left(E_{i+1,j+\frac{1}{2}}^{(q)} - E_{i,j+\frac{1}{2}}^{(q)} \right) \right],$$

where $\mathcal{F}_{\text{pot}}^h$ is the central-differencing approximation of \mathcal{F}_{pot} on the Yee mesh. It is easy to find that the associated free-energy change is minimized with

$$(3.13) \quad \eta = - \frac{E_{i+\frac{1}{2},j}^{(q)} - E_{i+\frac{1}{2},j+1}^{(q)} + E_{i+1,j+\frac{1}{2}}^{(q)} - E_{i,j+\frac{1}{2}}^{(q)}}{2}.$$

The second step of correction involves line shift for the electric field to further minimize the free energy [32, 26]. We follow the same idea that the flux entering and leaving each vertex should be kept the same. As depicted in Figure 2 (b), we increase electric fields on the b -th ($b = 0, \dots, N-1$) row by the same value η :

$$(3.14) \quad E_{i+\frac{1}{2},b}^{(q+1)} \leftarrow E_{i+\frac{1}{2},b}^{(q)} + \eta, \quad i = 0, \dots, N-1.$$

The associated free-energy change reads

$$\delta \mathcal{F}_{\text{pot}}^h[\eta] = \lambda^2 \eta^2 \frac{N}{2} + \lambda^2 \eta \sum_{i=1}^N E_{i+\frac{1}{2},b}^{(q)},$$

which has a unique minimizer

$$(3.15) \quad \eta = - \frac{\sum_{i=0}^{N-1} E_{i+\frac{1}{2},b}^{(q)}}{N}.$$

Similarly, we update the electric fields on the a -th ($a = 0, \dots, N-1$) column by

$$(3.16) \quad E_{a,j+\frac{1}{2}}^{(q+1)} \leftarrow E_{a,j+\frac{1}{2}}^{(q)} + \eta, \quad j = 0, \dots, N-1.$$

Then the minimizer of the associated free-energy change is given by

$$(3.17) \quad \eta = -\frac{\sum_{j=0}^{N-1} E_{a,j+\frac{1}{2}}^{(q)}}{N}.$$

It is stressed that the two local correction steps, (3.12), (3.14), and (3.16), are able to maintain the Gauss's law perfectly. Furthermore, the associated free-energy change is quadratic with an explicit expression for the minimizer. Therefore, the computational cost for each iteration step is linear.

Combining above steps described in sections 3.1, 3.2 and 3.3, we summarize the whole local Gauss's law preserving PIC (GP-PIC) method in Algorithm 3.1.

Algorithm 3.1 Local Gauss's Law Preserving PIC (GP-PIC) Method

Initial: $\mathbf{x}_p^m, \mathbf{v}_p^{m+1/2}, \mathbf{E}_h^m$, and tolerance τ

Update: $\mathbf{x}_p^{m+1}, \mathbf{v}_p^{m+3/2}, \mathbf{E}_h^{m+1}$

Step 1. Compute \mathbf{x}_p^{m+1} and get \mathbf{E}_h^*

for $p = 1$ to N_p **do**

 Update the x -component position with (3.4) and corresponding electric fields;

 Update the y -component position with (3.5) and corresponding electric fields;

end for

Step 2. Set $q = 0$ and $\mathbf{E}_h^{(0)} := \mathbf{E}_h^*$. Correct $\mathbf{E}_h^{(0)}$ to get \mathbf{E}_h^{m+1}

while the energy change $|\Delta \mathcal{F}_{\text{pot}}| \geq \tau$ **do**

for $i, j = 0$ to $N - 1$ **do**

 Update $\mathbf{E}_h^{(q)}$ by (3.12): $\mathbf{E}_h^{(q1)} \leftarrow \mathbf{E}_h^{(q)}$;

end for

for $b = 0$ to $N - 1$ **do**

 Update $\mathbf{E}_h^{(q1)}$ by (3.14): $\mathbf{E}_h^{(q2)} \leftarrow \mathbf{E}_h^{(q1)}$;

end for

for $a = 0$ to $N - 1$ **do**

 Update $\mathbf{E}_h^{(q2)}$ by (3.16): $\mathbf{E}_h^{(q+1)} \leftarrow \mathbf{E}_h^{(q2)}$;

end for

end while

Set $\mathbf{E}_h^{m+1} = \mathbf{E}_h^{(q+1)}$

Step 3. Compute \mathbf{v}_p^{m+1}

for $p = 1$ to N_p **do**

$$v_{p,x}^{m+\frac{3}{2}} = v_{p,x}^{m+\frac{1}{2}} - \Delta t E_{p,x}^{m+1}, \quad v_{p,y}^{m+\frac{3}{2}} = v_{p,y}^{m+\frac{1}{2}} - \Delta t E_{p,y}^{m+1}.$$

end for

THEOREM 3.1. *The proposed GP-PIC algorithm respects the discrete Gauss's law in the sense of*

$$\frac{E_{i+1/2,j}^{m+1} - E_{i-1/2,j}^{m+1}}{h} + \frac{E_{i,j+1/2}^{m+1} - E_{i,j-1/2}^{m+1}}{h} = \frac{n_0 - n_{i,j}^{m+1}}{\lambda^2},$$

provided that the Gauss's law at the previous time step holds:

$$\frac{E_{i+1/2,j}^m - E_{i-1/2,j}^m}{h} + \frac{E_{i,j+1/2}^m - E_{i,j-1/2}^m}{h} = \frac{n_0 - n_{i,j}^m}{\lambda^2}.$$

Proof. Let us check the Gauss's law at each vertex after each update. For Step 1 described in Section 3.2, we only check the case where the particle moves across the cell boundary. When the particle motion is within one cell, the proof is simpler and is omitted for brevity. With the motion as depicted in Figure 1 (c) and the update (3.6)-(3.11) in electric fields, the discrete Gauss's law at the node (i, j) becomes

$$\begin{aligned}
& \lambda^2 \frac{E_{i+1/2,j}^* - E_{i-1/2,j}^m}{h} + \lambda^2 \frac{E_{i,j+1/2}^m - E_{i,j-1/2}^m}{h} \\
&= \lambda^2 \frac{E_{i+1/2,j}^m - E_{i-1/2,j}^m}{h} + \lambda^2 \frac{E_{i,j+1/2}^m - E_{i,j-1/2}^m}{h} - \omega_p [-S_x(d_{x,i}^m)] S_y(d_{y,j}^m) \\
&= n_0 - n_{i,j}^m - \omega_p [-S_x(d_{x,i}^m)] S_y(d_{y,j}^m) \\
&= n_0 - [n_{i,j}^m + \Delta n_{i,j}],
\end{aligned}$$

where $\Delta n_{i,j}$ is the change of density at the point (i, j) when a particle moves from $\mathbf{x}_p^m = (x_{p,x}^m, x_{p,y}^m)$ to $(x_{p,x}^{m+1}, x_{p,y}^m)$. If $l = i + 1$, the discrete Gauss's law at the node $(i + 1, j)$ becomes

$$\begin{aligned}
& \lambda^2 \frac{E_{i+3/2,j}^* - E_{i+1/2,j}^*}{h} + \lambda^2 \frac{E_{i+1,j+1/2}^m - E_{i+1,j-1/2}^m}{h} \\
&= n_0 - n_{i+1,j}^m + w_p [S_x(d_{x,i+2}^{m+1}) - S_x(d_{x,i}^m)] S_y(d_{y,j}^m) \\
&= n_0 - n_{i+1,j}^m - w_p [S_x(d_{x,i+1}^{m+1}) - S_x(d_{x,i+1}^m)] S_y(d_{y,j}^m) \\
&= n_0 - [n_{i+1,j}^m + \Delta n_{i+1,j}],
\end{aligned}$$

where the identity $S_x(d_{x,i}^m) + S_x(d_{x,i+1}^m) = S_x(d_{x,i+1}^{m+1}) + S_x(d_{x,i+2}^{m+1})$ is used by the unity-integral property of the shape function. If $l > i + 1$, then $S_x(d_{x,i+1}^{m+1}) = 0$. The discrete Gauss's law at the node $(i + 1, j)$ becomes

$$\begin{aligned}
& \lambda^2 \frac{E_{i+3/2,j}^* - E_{i+1/2,j}^*}{h} + \lambda^2 \frac{E_{i+1,j+1/2}^m - E_{i+1,j-1/2}^m}{h} \\
&= n_0 - n_{i+1,j}^m - w_p [S_x(d_{x,i+1}^{m+1}) - S_x(d_{x,i+1}^m)] S_y(d_{y,j}^m) \\
&= n_0 - n_{i+1,j}^m - w_p [0 - S_x(d_{x,i+1}^m)] S_y(d_{y,j}^m) \\
&= n_0 - [n_{i+1,j}^m + \Delta n_{i+1,j}].
\end{aligned}$$

The discrete Gauss's laws at the nodes (r, j) , $r = i + 2, \dots, l - 1$ remain its form:

$$\begin{aligned}
& \lambda^2 \frac{E_{r+1/2,j}^* - E_{r-1/2,j}^*}{h} + \lambda^2 \frac{E_{r,j+1/2}^m - E_{r,j-1/2}^m}{h} \\
&= \lambda^2 \frac{E_{r+1/2,j}^m - E_{r-1/2,j}^m}{h} + \lambda^2 \frac{E_{r,j+1/2}^m - E_{r,j-1/2}^m}{h} \\
&= n_0 - n_{r,j}^m.
\end{aligned}$$

The Gauss's law at (l, j) becomes

$$\begin{aligned}
& \lambda^2 \frac{E_{l+1/2,j}^* - E_{l-1/2,j}^*}{h} + \lambda^2 \frac{E_{l,j+1/2}^m - E_{l,j-1/2}^m}{h} \\
&= n_0 - n_{l,j}^m + w_p [S_x(d_{x,l+1}^{m+1}) - S_x(d_{x,i}^m) - S_x(d_{x,i+1}^m)] S_y(d_{y,j}^m) \\
&= n_0 - n_{l,j}^m - w_p S_x(d_{x,l}^{m+1}) S_y(d_{y,j}^m) \\
&= n_0 - [n_{l,j}^m + \Delta n_{l,j}],
\end{aligned}$$

where $S_x(d_{x,i}^m) + S_x(d_{x,i+1}^m) = S_x(d_{x,l}^{m+1}) + S_x(d_{x,l+1}^{m+1})$ is used. The Gauss's law at the point $(l+1, j)$ becomes

$$\begin{aligned} & \lambda^2 \frac{E_{l+3/2,j}^m - E_{l+1/2,j}^*}{h} + \lambda^2 \frac{E_{l+1,j+1/2}^m - E_{l+1,j-1/2}^m}{h} \\ &= n_0 - n_{l+1,j}^m - \omega_p S_x(d_{x,l+1}^{m+1}) S_y(d_{y,j}^m) \\ &= n_0 - [n_{l+1,j}^m + \Delta n_{l+1,j}]. \end{aligned}$$

Thus, the electric field \mathbf{E}^* satisfies Gauss's law in Step 1. For the relaxation stage from \mathbf{E}^* to \mathbf{E}^{m+1} in Step 2, the Gauss's law preserving property is proved in [32]. In summary, the Gauss's law at each grid point is perfectly maintained in the whole GP-PIC method. \square

REMARK 3.1. *We remark that the relationship between the electric field and particle motion positions is not constrained by the leapfrog scheme, and therefore, the GP-PIC method constitutes a general framework applicable to other temporal discretization schemes. Also, the GP-PIC method can be coupled with other conservative schemes to achieve corresponding conservation properties. For example, energy conservation can be enforced by velocity correction [34], while asymptotic preserving strategies [33] can be adopted to deal with quasi-neutral limit. Moreover, by dimension splitting, the GP-PIC method can be directly extended to three dimensions.*

4. Numerical Results. To demonstrate the effectiveness of the proposed GP-PIC method, we conduct a series of 2D2V numerical experiments, including scenarios such as Landau damping, two-stream instability, and Diocotron instability. In this section, simulations are all performed on a computational domain $\Omega_{\mathbf{x}} = [0, L] \times [0, L]$ with periodic boundary conditions. To ensure the electro-neutrality condition required by the periodic boundary conditions, immobile ions are uniformly distributed in the background, i.e., only electrons are moving within the system.

We compare the GP-PIC results with those obtained by solving the Ampère equation and Poisson's equation for the update of the electric field. The “leapfrog” scheme is employed for computing particle motions among all methods. The method, labeled as “VA-PIC” in the following numerical tests, computes the electric field by Ampère's equation

$$(4.1) \quad \mathbf{E}_h^{m+1} = \mathbf{E}_h^m + \Delta t \left(-\mathbf{J}_h^{m+\frac{1}{2}} + \mathbf{Q} \right) / \lambda^2,$$

where we choose $\mathbf{Q} = 0$, $\mathbf{J}_h^{m+\frac{1}{2}} = \sum_{p=1}^{N_p} w_p S(\mathbf{x}_h - \mathbf{x}_p^{m+1/2}) \mathbf{v}_p^{m+1/2}$ with $\mathbf{x}_p^{m+1/2} = (\mathbf{x}_p^{m+1} + \mathbf{x}_p^m)/2$. Then, the electric field is further relaxed by using Step 2 in the algorithm to achieve the curl-free condition. Notice that the Gauss's law is not exactly satisfied due to the interpolation used in $\mathbf{J}_h^{m+\frac{1}{2}}$ when solving the Ampère's equation (4.1). However, this method, which computes the electric field through Ampère's equation, maintains the Gauss's law in Maxwell-Ampère Nernst-Planck equations [49, 50], as it inherently enforces the local charge conservation through direct resolution of the Nernst-Planck equation.

Alternatively, we can obtain the electric field being curl-free directly by solving the Poisson's equation for potential

$$(4.2) \quad -\lambda^2 \operatorname{grad}_h \cdot \operatorname{div}_h \phi^{m+1} = n_0 - n^{m+1},$$

where grad_h and div_h are obtained by using central differencing on the Yee mesh. Then, the electric field is calculated by $\mathbf{E}_h^{m+1} = -\operatorname{grad}_h \phi^{m+1}$, which clearly satisfies

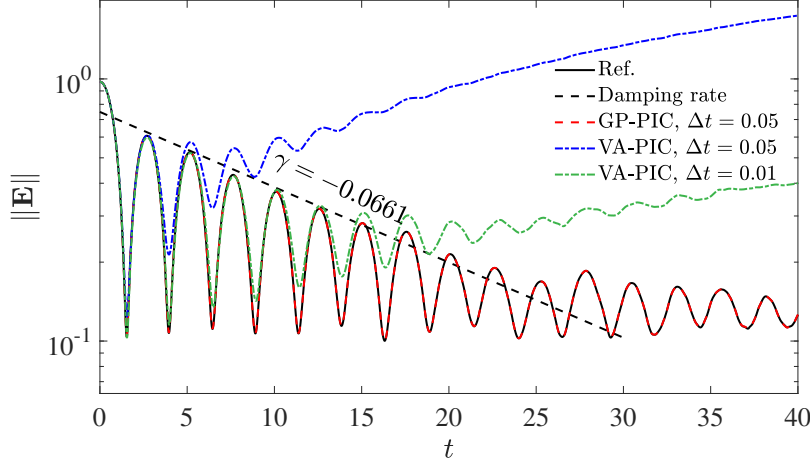


Fig. 3: The square root of electric energy in the simulation of Landau damping with different numerical methods. The reference solution, labeled as “Ref.” is obtained by solving the Poisson’s equation for the electric field with $\Delta t = 0.01$.

both the Gauss’s law and the curl-free condition with the accuracy dependent on the solver of the linear system (4.2). The GP-PIC method demonstrates inherent consistency with solutions from the Poisson’s equation due to its enforcement of Gauss’s law perfectly, despite the the accuracy of being curl-free being controlled by tolerance τ in the GP-PIC algorithm.

4.1. Landau damping. Landau damping is a widely tested PIC simulation [21, 3, 35, 42, 15]. We initialize the position and velocity of particles by sampling the distribution

$$f(\mathbf{x}, \mathbf{v}, t = 0) = \frac{1}{2\pi L^2} (1 + \alpha \cos(\mathbf{k} \cdot \mathbf{x})) e^{-\frac{v^2}{2}},$$

where $\alpha = 0.05$, $\mathbf{k} = (0.4, 0)^T$ and $L = 2\pi/0.4$. We choose the mesh size $N_x = N_y = 32$ and the number of particle $N_p = 6.4 \times 10^5$. The solution obtained by solving the Poisson’s equation for the electric field with a time step $\Delta t = 0.01$ serves as the reference solution. It is compared with the results obtained from our local method and solving the Ampère’s equation with a timestep $\Delta t = 0.05$. In Figure 3, we present the evolution of the square root of the electric energy given by

$$\|\mathbf{E}\| = \left[\sum_{i,j}^{N^2} h^2 \left(|E_{i+\frac{1}{2},j}|^2 + |E_{i,j+\frac{1}{2}}|^2 \right) \right]^{\frac{1}{2}},$$

using the three different methods. The square of electric energy shown in Figure 3 demonstrates that the results from our new methods agree with the reference solution very well and show a damping rate close to $\gamma = -0.0661$ that is predicted by theory [35]. In contrast, the result computed by the Ampère’s equation, which may not satisfy the Gauss’s law, exhibits relatively large errors, especially in late stage of long-term simulations. Its performance can be significantly improved with smaller time

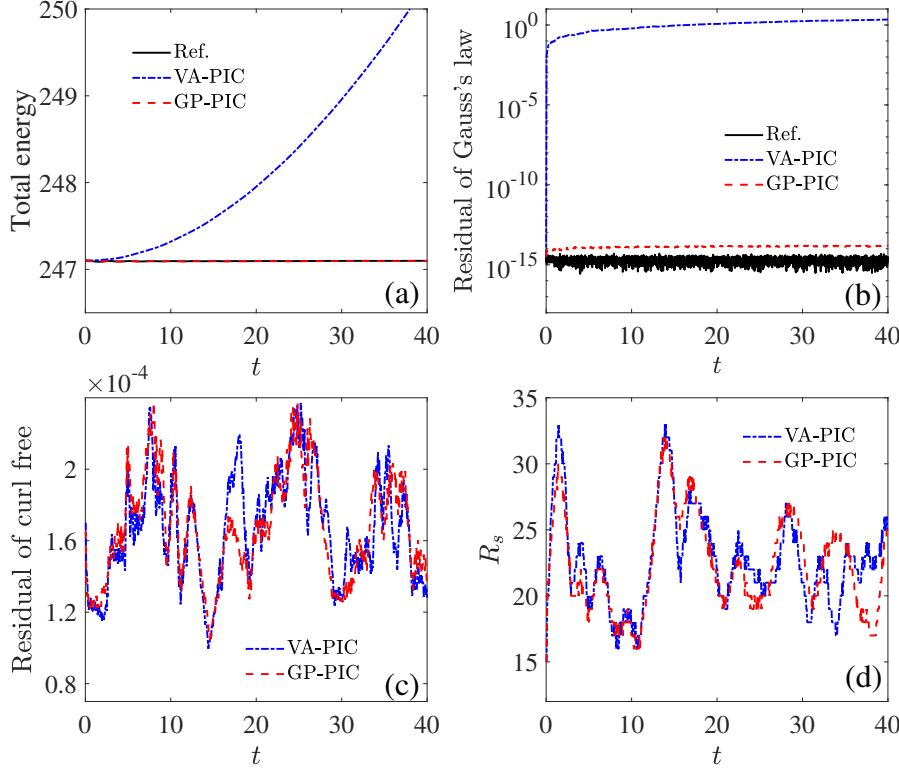


Fig. 4: Simulation results for the case of the Landau damping with $\Delta t = 0.05$ and $\tau = 10^{-7}$: (a) the total energy; (b) the residual error of the Gauss's law; (c) the residual error of the curl-free condition; (d) The number of iteration steps, R_s , used in relaxation stage.

stepsizes, but remaining worse than the Gauss's law satisfying schemes for long time. These results demonstrate the importance of maintaining the Gauss's law during the simulations.

Figure 4 presents the performance of the methods in preserving the total energy, the Gauss's law, the curl-free condition in terms of residual errors and the number of iteration steps used in the correction stage. The total energy is discretized by

$$F = \frac{\lambda^2}{2} \|\mathbf{E}\|^2 + \sum_{p=1}^{N_p} \omega_p \frac{v_p^2}{2}.$$

Although we have not theoretically establish the energy conservation for the proposed local method, Figure 4 (a) demonstrates that the total energy is preserved as well as the results obtained by the Poisson's equation. In contrast, the total energy obtained by the Ampère's equation keeps growing in the simulations. In terms of energy conservation, the energy-conserving correction strategies [34] can be combined to improve the performance of the numerical methods. From Figure 4 (b), one can observe that

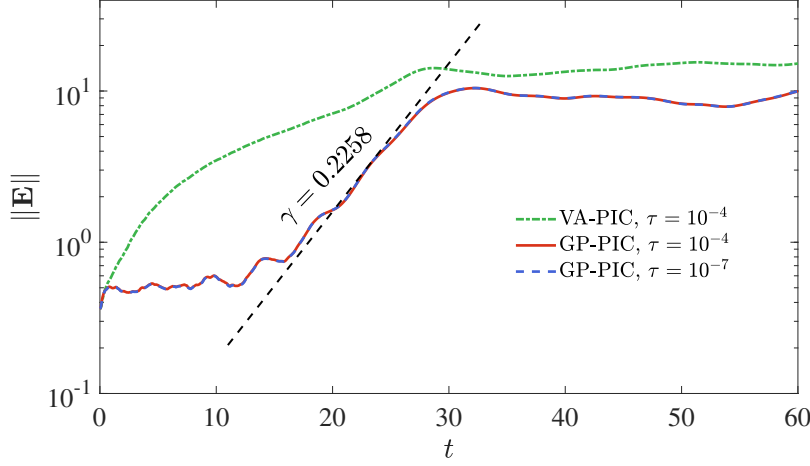


Fig. 5: The square root of electric energy in the simulation of two-stream instability with $\Delta t = 0.05$. The black dashed line represents a theoretical growth rate $\gamma = 0.2258$. Two different stopping criteria $\tau = 10^{-4}$ and $\tau = 10^{-7}$ are considered in the curl-free relaxation stage.

the residual errors of the Gauss's law for the electric field obtained from the proposed local method and Poisson's equation are both close to the machine precision, due to round-off error. However, the residual error of the Gauss's law computed by the Ampère's equation increase significantly in simulations. As the electric field calculated using Poisson's equation with Yee mesh strictly satisfies the curl-free condition, we have omitted the Poisson's results in Figure 4 (c). The residual error of curl free calculated by the proposed local method and the Ampère's equation increases in initial a few steps and is well controlled in the entire simulations via the stopping criterion $\tau = 10^{-7}$ we set in both algorithms. By setting the same stopping criterion, the iteration steps in the correction stage are on the same level for GP-PIC method and VA-PIC method as displayed in Figure 4 (d).

4.2. Two-stream instability. Two-stream instability is a typical phenomenon that has been well investigated by many studies [3, 15, 42, 55]. In the two-stream instability test, two beams of particles, each with an average velocity in opposite directions, move through space. Such a plasma system is inherently unstable and these two beams eventually merge to form a vortex structure. During the simulation, energy gradually transfers from the particles to the electric field, resulting in a decrease in kinetic energy and an increase in electric energy. The initial particle position and velocity is obtained by sampling the distribution

$$f(\mathbf{x}, \mathbf{v}, t = 0) = \frac{1}{2\pi L^2} (1 + \alpha \cos(\mathbf{k} \cdot \mathbf{x})) \left[\frac{1}{2} e^{-\frac{(\mathbf{v} - \mathbf{v}_d)^2}{2}} + \frac{1}{2} e^{-\frac{(\mathbf{v} + \mathbf{v}_d)^2}{2}} \right],$$

where $\alpha = 0.003$, $\mathbf{k} = (0.2, 0)^T$, $L = 2\pi/0.2$ and $\mathbf{v}_d = (2.4, 0)^T$. We choose the mesh size $N_x = N_y = 64$ and number of particle $N_p = 6.4 \times 10^5$. The square root of electric energy is displayed in Figure 5, which reveals that the proposed local Gauss's law preserving method is consistent with previous works [42], with a theoretical growth

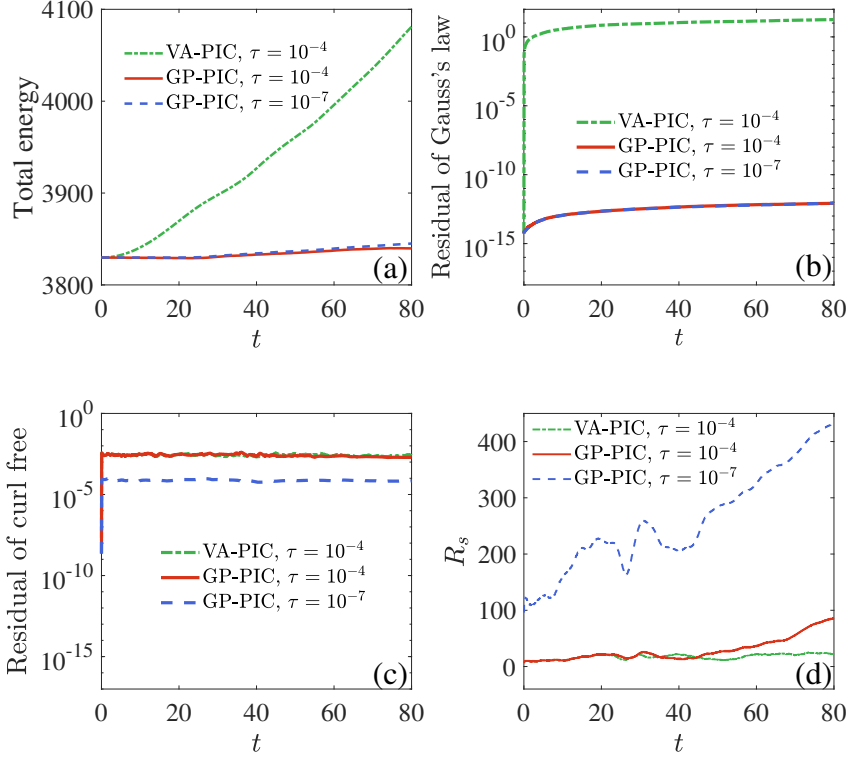


Fig. 6: Simulation results for the case of the two-stream instability with $\Delta t = 0.05$: (a) the total energy; (b) the residual error of the Gauss's law; (c) the residual error of the curl-free condition; (d) The number of iteration steps, R_s , used in relaxation stage.

rate of electric energy being $\gamma = 0.2258$. Note that our proposed GP-PIC method agrees well with Poisson's result, so we omit the figures of Poisson's result in this example.

Figure 6 displays the total energy, the residual error of the Gauss's law, curl-free condition, and the number of relaxation steps in the correction stage. We observe the similar results as Landau damping that the total energy computed by VA-PIC method deviates significantly from the initial energy as time evolves, whereas our proposed GP-PIC method exhibits significantly smaller deviations, displayed in Figure 6 (a). As previously discussed, while energy-conserving scheme can indeed be designed, its rigorous implementation lies beyond the scope of this work. From Figure 6 (b), one can find that the Gauss's law is perfectly satisfied in the proposed local methods. However, it is not true for the results obtained by the Ampère's equation. To test the effect of the stopping criteria τ , we perform simulations with $\tau = 10^{-4}$ and $\tau = 10^{-7}$. It is of interest to find that with a more stringent stopping criterion τ , the residual error of the Gauss's law does not change much, as expected. But the number of

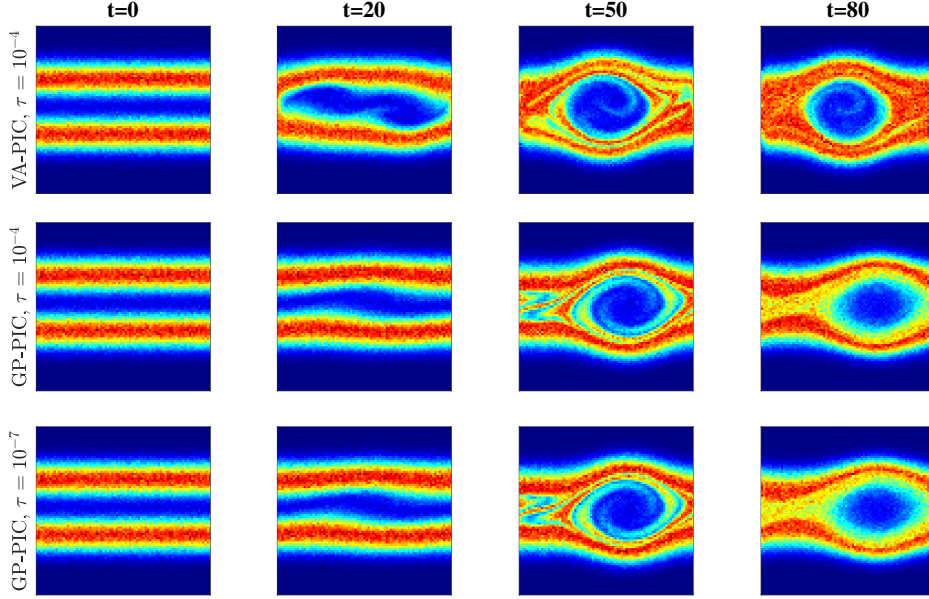


Fig. 7: The $x - v_x$ phase space distribution for the case of two-stream instability with $\lambda = 1$ and $\Delta t = 0.05$ at time $t = 0, 20, 50, 80$. The first row shows the results computed by the Ampère's equation. The second row ($\tau = 10^{-4}$) and the third row ($\tau = 10^{-7}$) are obtained by the proposed method with different stopping criteria in the correction stage.

iteration steps, R_s , in the correction stage of the proposed algorithm increases and the residual error of the curl-free condition effectively reduces one order of magnitude, as revealed by Figure 6 (c) and (d).

As shown in Figure 7, we also study the $x-v_x$ phase space distribution of the system with different methods. A violation of the Gauss's law results in a prominent error accumulation for long-term simulations, as revealed by the results obtained from the Ampère's equation in the first row of Figure 7. The phase space distribution exhibits vortex structures that are significantly different from those obtained using the local method. Furthermore, the phase space distribution does not change much with a more stringent stopping criterion τ , indicating that the curl-free condition is not as crucial as the Gauss's law in long-term simulations.

4.3. Diocotron instability. Finally, we perform a variation of Diocotron instability to study the electron vortices when exposed to an external magnetic field. This instability has been well studied numerically in many works [20, 53, 22, 54]. The initial electron distribution follows

$$f(x, y, \mathbf{v}, t = 0) = \frac{C}{2\pi} e^{-\frac{v^2}{2}} e^{-\frac{(x-L/4)^2}{2(\delta L)^2}}, \quad r = \sqrt{(x - L/2)^2 + (y - L/2)^2},$$

where $\delta = 0.03$, $L = 22$ and C is a normalization parameter. Here, a uniform magnetic field $\mathbf{B} = (0, 0, B_z)$ is imposed, and we choose $B_z = 5$ and $B_z = 15$. The mesh size

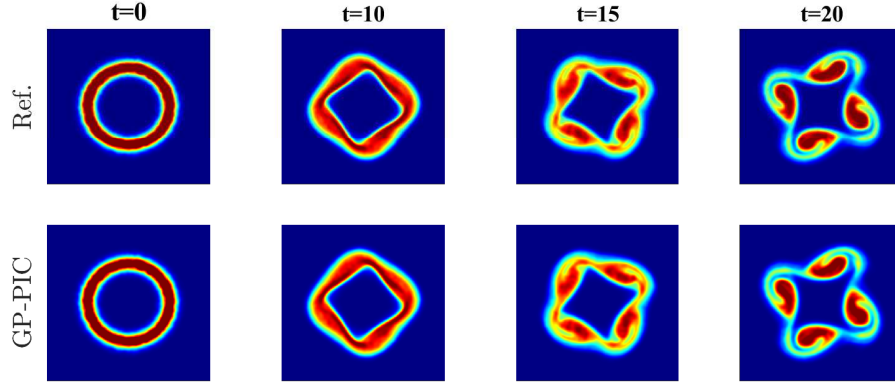


Fig. 8: The distribution of electron in the case of Diocotron instability at time $t = 0, 10, 15, 20$ with $B_z = 5$. The reference solution, labeled as “Ref.” is obtained by solving the Poisson’s equation for the electric field.

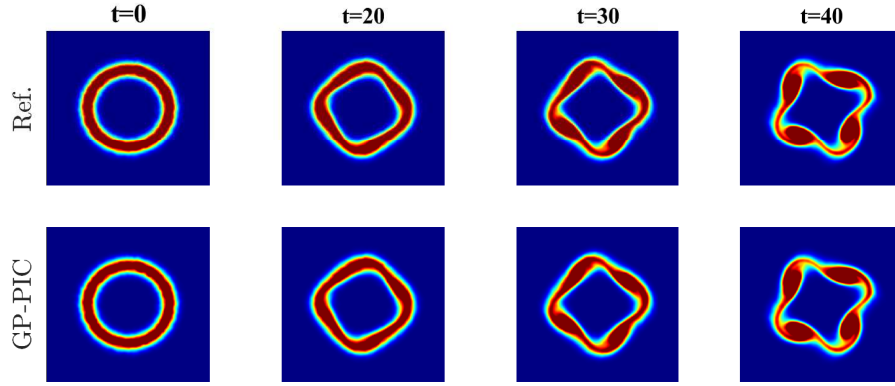


Fig. 9: The distribution of electron in the case of Diocotron instability at time $t = 0, 20, 30, 40$ with $B_z = 15$. The reference solution, labeled as “Ref.” is obtained by solving the Poisson’s equation for the electric field.

is $N_x = N_y = 64$, timestep is $\Delta t = 0.01$ and the number of particles is taken as $N_p = 10^6$ in the simulation. In this case, with finite-size particle approximation (2.8) for the distribution function, the motions of electron follow

$$(4.3) \quad \frac{d\mathbf{x}_p}{dt} = \mathbf{v}_p,$$

$$(4.4) \quad \frac{d\mathbf{v}_p}{dt} = -[\mathbf{E}(\mathbf{x}_p) + \mathbf{v}_p \wedge \mathbf{B}],$$

for $p = 1, \dots, N_p$.

As evidenced by Figure 8 and Figure 9, the proposed method can effectively capture a vortex structure of the electron distribution due to the magnetic field in the z -direction. By setting $B_z = 5$ in Figure 8, four well-resolved vortex structures

emerge prominently in the simulation at $t = 20$. When the strength of magnetic field is increased to $B_z = 15$ in Figure 9, it takes longer time to form vortex structures, being consistent with the results reported in the work [53]. Furthermore, the vortices exhibit diminished features compared to the $B_z = 5$ configuration, a phenomenon demonstrated in [22].

5. Conclusions. The importance of rigorously maintaining the Gauss’s law in plasma simulations cannot be overemphasized. This work has proposed a Gauss’s law preserving method for the electric field updating in particle-in-cell simulations in the electrostatic limit. The proposed method updates the electric field locally according to the electric fluxes induced by particle motion through splitting the motion into sub-steps along each dimension of the computational mesh, resulting a method that can enforce the Gauss’s law exactly. To obtain a curl-free electric field, a local update scheme has been developed to further correct the electric field by relaxing the electric-field free energy subject to the Gauss’s law. Theoretical analysis has confirmed that the proposed method maintains the Gauss’s law up to round-off precision. Numerical performance on classical benchmarks, including the Landau damping, two-stream instability and Diocotron instability, has evidenced the advantages of the proposed method. It is expected that the local nature of the proposed method makes it a promising tool in parallel simulations of large-scale plasma. In addition, the feature that electric fields are locally updated according to the electric fluxes induced by particle motion can be further employed to construct a fully implicit discretization that allows a large time stepping size, which has great potential in efficient simulations of the quasineutral cases.

Acknowledgements. This work is supported by the CAS AMSS-PolyU Joint Laboratory of Applied Mathematics (Grant No. JLFS/P-501/24). Z. Qiao is partially supported by the Hong Kong Research Grants Council RFS grant RFS2021-5S03, NSFC/RGC Joint Research Scheme N_PolyU5145/24, GRF grants 15302122 and 15305624. Q. Yin is partially supported by the Hong Kong Polytechnic University Postdoc Matching Fund Scheme 4-W425. The work of Z. Xu is partially supported by NSFC (grants No. 12325113 and 12426304) and National Key R&D Program of China (grant No. 2024YFA1012403). The work of S. Zhou is partially supported by National Key R&D Program of China 2023YFF1204200.

REFERENCES

- [1] S. E. Anderson, W. T. Taitano, L. Chacón, and A. N. Simakov. An efficient, conservative, time-implicit solver for the fully kinetic arbitrary-species 1D-2V Vlasov-Ampère system. *J. Comput. Phys.*, 419:109686, 2020.
- [2] M. Baptista, R. Schmitz, and B. Dünweg. Simple and robust solver for the Poisson-Boltzmann equation. *Phys. Rev. E*, 80:016705, 2009.
- [3] N. Besse and E. Sonnendrücker. Semi-Lagrangian schemes for the Vlasov equation on an unstructured mesh of phase space. *J. Comput. Phys.*, 191(2):341–376, 2003.
- [4] C. K. Birdsall and A. B. Langdon. *Plasma physics via computer simulation*. CRC press, 2018.
- [5] J. P. Boris. Relativistic plasma simulation-optimization of a hybrid code. In *Proc. Fourth Conf. Num. Sim. Plasmas*, pages 3–67, 1970.
- [6] L. Chacón and G. Chen. A curvilinear, fully implicit, conservative electromagnetic PIC algorithm in multiple dimensions. *J. Comput. Phys.*, 316:578–597, 2016.
- [7] G. Chen and L. Chacón. A multi-dimensional, energy-and charge-conserving, nonlinearly implicit, electromagnetic Vlasov–Darwin particle-in-cell algorithm. *Comput. Phys. Commun.*, 197:73–87, 2015.
- [8] G. Chen, L. Chacón, and D. C. Barnes. An energy- and charge-conserving, implicit, electrostatic particle-in-cell algorithm. *J. Comput. Phys.*, 230(18):7018–7036, 2011.

- [9] G. Chen, L. Chacón, L. Yin, B. J. Albright, D. J. Stark, and R. F. Bird. A semi-implicit, energy-and charge-conserving particle-in-cell algorithm for the relativistic Vlasov-Maxwell equations. *J. Comput. Phys.*, 407:109228, 2020.
- [10] Y. Chen and G. Tóth. Gauss’s law satisfying energy-conserving semi-implicit particle-in-cell method. *J. Comput. Phys.*, 386:632–652, 2019.
- [11] Y. Cheng, A. J. Christlieb, and X. Zhong. Energy-conserving discontinuous Galerkin methods for the Vlasov–Ampère system. *J. Comput. Phys.*, 256:630–655, 2014.
- [12] B. I. Cohen, A. B. Langdon, and A. Friedman. Implicit time integration for plasma simulation. *J. Comput. Phys.*, 46(1):15–38, 1982.
- [13] G. Colonna and A. D’Angola. *Plasma Modeling: Methods and Applications*. IOP Publishing, 2022.
- [14] G.-H. Cottet and P.-A. Raviart. Particle methods for the one-dimensional Vlasov–Poisson equations. *SIAM J. Numer. Anal.*, 21(1):52–76, 1984.
- [15] N. Crouseilles, G. Lattu, and E. Sonnendrücker. A parallel Vlasov solver based on local cubic spline interpolation on patches. *J. Comput. Phys.*, 228(5):1429–1446, 2009.
- [16] P. Degond, F. Deluzet, L. Navoret, A.-B. Sun, and M.-H. Vignal. Asymptotic-preserving Particle-In-Cell method for the Vlasov–Poisson system near quasineutrality. *J. Comput. Phys.*, 229(16):5630–5652, 2010.
- [17] F. Fahrenberger and C. Holm. Computing the Coulomb interaction in inhomogeneous dielectric media via a local electrostatics lattice algorithm. *Phys. Rev. E*, 90(6):063304, 2014.
- [18] F. Fahrenberger, Z. Xu, and C. Holm. Simulation of electric double layers around charged colloids in aqueous solution of variable permittivity. *J. Chem. Phys.*, 141(6):064902, 2014.
- [19] F. Filbet. Convergence of a finite volume scheme for the Vlasov–Poisson system. *SIAM J. Numer. Anal.*, 39(4):1146–1169, 2001.
- [20] F. Filbet and L. M. Rodrigues. Asymptotically stable particle-in-cell methods for the Vlasov–Poisson system with a strong external magnetic field. *SIAM J. Numer. Anal.*, 54(2):1120–1146, 2016.
- [21] F. Filbet, E. Sonnendrücker, and P. Bertrand. Conservative numerical schemes for the Vlasov equation. *J. Comput. Phys.*, 172(1):166–187, 2001.
- [22] A. Gu, Y. He, and Y. Sun. Hamiltonian Particle-in-Cell methods for Vlasov–Poisson equations. *J. Comput. Phys.*, 467:111472, 2022.
- [23] W. Guo and J.-M. Qiu. A conservative low rank tensor method for the Vlasov dynamics. *SIAM J. Sci. Comput.*, 46(1):A232–A263, 2024.
- [24] G. J. M. Hagelaar and L. C. Pitchford. Solving the Boltzmann equation to obtain electron transport coefficients and rate coefficients for fluid models. *Plasma Sources Sci. Technol.*, 14(4):722–733, 2005.
- [25] L. Ji, Z. Yang, Z. Li, D. Wu, S. Jin, and Z. Xu. An asymptotic-preserving and energy-conserving particle-in-cell method for Vlasov–Maxwell equations. *J. Math. Phys.*, 64(6):063503, 2023.
- [26] J. Jiang and Z. Wang. Improved local lattice monte carlo simulation for charged systems. *J. Chem. Phys.*, 148(11):114105, 2018.
- [27] M. Kirchhart and R. P. Wilhelm. The numerical flow iteration for the Vlasov–Poisson equation. *SIAM J. Sci. Comput.*, 46(3):A1972–A1997, 2024.
- [28] K. Kormann and E. Sonnendrücker. A dual grid geometric electromagnetic particle in cell method. *SIAM J. Sci. Comput.*, 46(5):B621–B646, 2024.
- [29] A. B. Langdon. On enforcing Gauss’ law in electromagnetic particle-in-cell codes. *Comput. Phys. Commun.*, 70(3):447–450, 1992.
- [30] G. Lapenta. Kinetic plasma simulation: Particle in cell method. *XII Carolus Magnus Summer School on Plasma and Fusion Energy Physics*, pages 76–85, 2015.
- [31] G. Lapenta. Exactly energy conserving semi-implicit particle in cell formulation. *J. Comput. Phys.*, 334:349–366, 2017.
- [32] B. Li, Q. Yin, and S. Zhou. Finite-difference approximations and local algorithm for the Poisson and Poisson-Boltzmann electrostatics. *arXiv preprint arXiv:2409.15796*, 2024.
- [33] Z. Li, Z. Xu, and Z. Yang. An energy-conserving Fourier particle-in-cell method with asymptotic-preserving preconditioner for Vlasov-Ampère system with exact curl-free constraint. *J. Comput. Phys.*, 495:112529, 2023.
- [34] J. Liang, Z. Xu, and Y. Zhao. Energy stable scheme for random batch molecular dynamics. *J. Chem. Phys.*, 160(3):034101, 2024.
- [35] C. Liu and K. Xu. A unified gas kinetic scheme for continuum and rarefied flows v: Multiscale and multi-component plasma transport. *Commun. Comput. Phys.*, 22(5):1175–1223, 2017.
- [36] H. Liu, X. Cai, Y. Cao, and G. Lapenta. An efficient energy conserving semi-Lagrangian kinetic scheme for the Vlasov-Ampère system. *J. Comput. Phys.*, 492:112412, 2023.
- [37] A. C. Maggs. Dynamics of a local algorithm for simulating Coulomb interactions. *J. Chem.*

- Phys.*, 117(5):1975–1981, 2002.
- [38] A. C. Maggs and V. Rossetto. Local simulation algorithms for Coulomb interactions. *Phys. Rev. Lett.*, 88:196402, 2002.
 - [39] P. J. Mardahl and J. P. Verboncoeur. Charge conservation in electromagnetic PIC codes; spectral comparison of Boris/DADI and Langdon-Marder methods. *Comput. Phys. Commun.*, 106(3):219–229, 1997.
 - [40] B. Marder. A method for incorporating Gauss’ law into electromagnetic PIC codes. *J. Comput. Phys.*, 68(1):48–55, 1987.
 - [41] R. J. Mason. Implicit moment particle simulation of plasmas. *J. Comput. Phys.*, 41(2):233–244, 1981.
 - [42] A. Medaglia, L. Pareschi, and M. Zanella. Stochastic Galerkin particle methods for kinetic equations of plasmas with uncertainties. *J. Comput. Phys.*, 479:112011, 2023.
 - [43] R. L. Morse and C. W. Nielson. Numerical simulation of the weibel instability in one and two dimensions. *Phys. Fluids*, 14:830–840, 1971.
 - [44] B. J. Muga and J. F. Wilson. Particle-in-cell method. In *Dynamic Analysis of Ocean Structures*, pages 105–116. Springer, 1970.
 - [45] C.-D. Munz, P. Omnes, R. Schneider, E. Sonnendrücker, and U. Voss. Divergence correction techniques for Maxwell solvers based on a hyperbolic model. *J. Comput. Phys.*, 161(2):484–511, 2000.
 - [46] A. Myers, P. Colella, and B. V. Straalen. A 4th-order particle-in-cell method with phase-space remapping for the Vlasov–Poisson equation. *SIAM J. Sci. Comput.*, 39(3):B467–B485, 2017.
 - [47] I. Pasichnyk and B. Dünweg. Coulomb interactions via local dynamics: A molecular-dynamics algorithm. *J. Phys: Condens. Matter*, 16:S3999, 2004.
 - [48] M. C. Pinto and F. Charles. Uniform convergence of a linearly transformed particle method for the Vlasov–Poisson system. *SIAM J. Numer. Anal.*, 54(1):137–160, 2016.
 - [49] Z. Qiao, Z. Xu, Q. Yin, and S. Zhou. A Maxwell–Ampère Nernst–Planck framework for modeling charge dynamics. *SIAM J. Appl. Math.*, 83(2):374–393, 2023.
 - [50] Z. Qiao, Z. Xu, Q. Yin, and S. Zhou. Structure-preserving numerical method for Maxwell–Ampère Nernst–Planck model. *J. Comput. Phys.*, 475:111845, 2023.
 - [51] Z. Qiao, Z. Xu, Q. Yin, and S. Zhou. Local structure-preserving relaxation method for equilibrium of charged systems on unstructured meshes. *SIAM J. Sci. Comput.*, 46(4):A2248–A2269, 2024.
 - [52] J.-M. Qiu and C.-W. Shu. Conservative Semi-Lagrangian finite difference WENO formulations with applications to the Vlasov equation. *Commun. Comput. Phys.*, 10(4):979–1000, 2011.
 - [53] L. F. Ricketson and A. J. Cerfon. Sparse grid techniques for particle-in-cell schemes. *Plasma Phys. Control. Fusion*, 59(2):024002, 2016.
 - [54] L. F. Ricketson and G. Chen. A pseudospectral implicit particle-in-cell method with exact energy and charge conservation. *Comput. Phys. Commun.*, 291:108811, 2023.
 - [55] L. F. Ricketson and J. Hu. An explicit, energy-conserving particle-in-cell scheme. *arXiv preprint arXiv:2411.09605*, 2024.
 - [56] J. Rottler and A. C. Maggs. A continuum, $O(N)$ Monte Carlo algorithm for charged particles. *J. Chem. Phys.*, 120(7):3119–3129, 2004.
 - [57] J. Rottler and A. C. Maggs. Local molecular dynamics with Coulombic interactions. *Phys. Rev. Lett.*, 93(17):170201, 2004.
 - [58] I. V. Sokolov. Alternating-order interpolation in a charge-conserving scheme for particle-in-cell simulations. *Comput. Phys. Commun.*, 184(2):320–328, 2013.
 - [59] A. Taflove, K.R. Umashankar, B. Beker, F. Harfoush, and K. S. Yee. Detailed FD-TD analysis of electromagnetic fields penetrating narrow slots and lapped joints in thick conducting screens. *IEEE Trans. Antennas Propagat.*, 36:247–257, 1988.
 - [60] W. T. Taitano, J. W. Burby, and A. Alekseenko. A conditional formulation of the Vlasov–Ampère equations: A conservative, positivity, asymptotic, and Gauss law preserving scheme. *arXiv preprint arXiv:2410.20106*, 2024.
 - [61] J. Villasenor and O. Buneman. Rigorous charge conservation for local electromagnetic field solvers. *Comput. Phys. Commun.*, 69(2-3):306–316, 1992.
 - [62] B. Wang, G. H. Miller, and P. Colella. A particle-in-cell method with adaptive phase-space remapping for kinetic plasmas. *SIAM J. Sci. Comput.*, 33(6):3509–3537, 2011.
 - [63] K. Yee. Numerical solution of initial boundary value problems involving Maxwell’s equations in isotropic media. *IEEE Trans. Antennas Propagat.*, 14(3):302–307, 1966.
 - [64] S. Zhou, Z. Wang, and B. Li. Mean-field description of ionic size effects with non-uniform ionic sizes: A numerical approach. *Phys. Rev. E*, 84:021901, 2011.